International Journal of Heat and Mass Transfer 208 (2023) 124056

Contents lists available at ScienceDirect

International Journal of Heat and Mass Transfer

journal homepage: www.elsevier.com/locate/hmt

The mechanism of enhanced photothermal conversion of low-dimensional plasmonic nanofluids with LFPs resonance

Rui Yang[a], Xiaoke Li[a,b,*], Fei Yin[c], Jinwen Shi[b], Dengwei Jing[b,*]

[a] College of Materials and Chemistry & Chemical Engineering, Chengdu University of Technology, Chengdu 610059, China
[b] International Research Center for Renewable Energy, State Key Laboratory of Multiphase Flow in Power Engineering, Xi'an Jiaotong University, Xi'an 710049, China
[c] State Key Laboratory of Oil and Gas Reservoir Geology and Exploitation, Chengdu University of Technology, Chengdu 610059, China

ARTICLE INFO

Article history:
Received 8 December 2022
Revised 16 February 2023
Accepted 3 March 2023

Keywords:
Plasmonic nanofluids
Low-frequency phonon resonance
Photothermal conversion
Low-dimensional materials

ABSTRACT

Solar-thermal utilization is one of the important ways of energy utilization at present and in the future. Nanofluids play a key role in photothermal conversion. In this work, the low-dimensional plasmonic TiN/MWCNTs nanofluids were firstly proposed. The photothermal conversion properties of low-dimensional plasmonic nanofluids was systematically investigated. The analytical results indicated that the heat transfer and optical properties of plasmonic nanofluids were significantly enhanced. Specifically, thanks to the expanded light absorption by the LSPR of nano-TiN and the enhanced thermal transport by its low-frequency phonon (LFP) resonance with MWCNTs, the photothermal conversion efficiency can reach 68.1% with 10 ppm TiN/MWCNTs nanofluids, which was 22.9% higher than that of the MWCNTs nanofluids. And the photothermal conversion efficiency of TiN/MWCNTs nanofluids (40 ppm) reached 76.4%. Furthermore, through the simulation and experimental results, this paper explained the mechanism of the enhanced solar-thermal conversion performance of nanofluids from the perspective of phonon heat transfer.

1. Introduction

The use of clean and renewable energy has emerged the future direction of development in the world [1]. Solar energy has been one of the most promising renewable energy sources due to its sustainability and environmental friendliness [2]. So far, solar energy has been utilized mainly in the form of photovoltaic (PV) [3], photochemical conversion [4], and photothermal conversion. And photothermal conversion is one of simplest forms of solar utilizations [5]. The selection of the working medium is critical in light to heat process. However, the traditional working mediums (water, thermal oil, etc.) cannot meet the current heat transfer demand gradually [6].

For this reason, investigators have done a lot of work to improve the heat collection efficiency [7,8]. Nanofluid is a novel heat transfer media [9], which is prepared by formulating nano particles into conventional working media to form a homogeneous fluid. Due to the excellent heat transfer properties, nanofluids can be used in various fields, including desalination [10], machining [11], heating [12], thermal exchangers [13], and solar collectors [14,15].

Recently, the plasmonic nanofluids based on localized surface plasmon resonance (LSPR) nanoparticles have been noticed in the field of solar thermal applications. The LSPR phenomenon appears when plasmonic nanoparticles are excited by light at specific wavelengths, which could cause collective oscillation of free electrons, and then leading to significant enhancement of their own absorption and scattering of light [16]. In particular, when plasma is integrated into solar technology, it achieves ultra-broadband of solar energy absorption since it provides significant potential for size-, shape- and coupling-driven spectral structuring and adjustments of material absorption behavior [17]. It has been found that plasmonic nanofluids can enhance the light absorption intensity of the heat-conducting fluids at specific wavelengths with pretty low concentration effectively [18]. Wen's group prepared plasmonic nanofluids by using silver (Ag) nanoparticles [19]. It was found that only 6.5 ppm of nanofluids were required to increase the heat captured by solar collectors by 144%. The team also studied the photothermal application process of gold (Au) nanofluids [20]. The photothermal conversion efficiency was found to increase with increasing mass concentration, but in a non-linear manner.

Abbreviations: TiN, Titanium nitride; MWCNTs, Multi-walled carbon nanotubes; LSPR, Localized surface plasmon resonance; LFP, Low-frequency phonon; ITT, Interfacial thermal transport; EG, Ethylene glycol; PCe, Photothermal conversion efficiency; EM, Electromagnetic; HV, Horizontal vibration; VV, Vertical vibration.

* Corresponding authors at: Xiaoke Li and Dengwei Jing, Postal address: No.1, Dongsan Road, Erxianqiao, Chenghua District, Chengdu 610059, China.
E-mail address: dwjing@mail.xjtu.edu.cn (D. Jing).

https://doi.org/10.1016/j.ijheatmasstransfer.2023.124056
0017-9310/

Nomenclature

r	The radius of the TiN nanoparticles
a	The shape coefficient
m	The optical constants
$I_{AM1.5}$	The standard solar radiation spectrum
η	The photo-thermal conversion efficiency
m	The mass of working fluids
c_p	The constant-pressure heat capacities of working fluids
E_η	The experimental uncertainty
δ	The particle spacing

Mallah et al. [21] prepared the plasmonic nanofluids with mixed Ag nanoparticles and found that the efficiency of solar collectors could be enhanced by about 85% with only 0.001 wt.% concentration. However, the high price of precious metals has certain limitations in industrial applications, so it is urgent to find or design new nanomaterials with both good economy and high performance.

It has been demonstrated that titanium nitride (TiN) nanoparticles have the similar LSPR effect of noble metals nanoparticles with mature production technology and low cost [22,23]. Wang et al. [24] showed that TiN nanoparticles can absorb a wide range of visible and near-infrared light compared to carbon nanotubes, Ag, Au, graphene, and metal sulfides. It indicated that TiN nanoparticles can produce LSPR effects in visible light and longer wavelengths, but its absorption peak was narrow so the single-component TiN nanofluids often cannot be well regulated or achieve wide-domain absorption [25]. And the scattering of solar photon energy from ultraviolet (UV) to deep infrared (IR) is so significant that almost no single material or structure can collect all of its portion. Therefore, it remains a challenge to make nanofluids based on nano-TiN to have more abundant application scenarios in the solar thermal conversion process.

As a result, researchers have compounded two (or more) nanoparticles to synthesis the hybrid nanofluids and then exploiting the interparticle coupling effects to improve deficiencies in the thermal network, stability or photo-thermal properties of nanofluids. The hybrid nanofluids can provide the potential to match the solar radiation spectrum and consequently achieve broadband solar thermo-absorption on the basis of the complementary optical absorption properties of the different nanoparticles [26,27]. Some scholars have already investigated the photothermal conversion of hybrid plasmonic nanofluids such as Ag@TiO_2 [28], Au/SiO_2 [29], Ag-Au [30] nanofluids etc. Furthermore, The solar-thermal conversion of Au/TiN nanofluids was investigated by Wang et al. [31]. The light absorption capacity of the hybrid nanofluids was enhanced due to the superposition of the dual plasmon resonance effect.

Meanwhile, the heat transfer properties of nanoparticles are also one of the crucial factors in determining the efficiency of light to heat conversion. The phonon refers the quantized energy of lattice vibrations. The phonon heat transfer is the main mechanism of heat transfer in most carbon based materials [32]. The multi-walled carbon nanotubes (MWCNTs), as a kind of one-dimensional nanomaterials, are crystalline materials with tightly arranged carbon (C) atoms, and their regular crystal structure and sp^2 structure of carbon atoms have excellent conductivity for phonons. Therefore, MWCNTs have a relatively outstanding axial thermal conductivity. However, at the microscopic level, the transport properties of phonons at the interface are distinct compared to those in the nanoscale region. The different phonon transport modes of the components in the hybrid materials lead to the interface being the main region of phonon scattering [33]. This phenomenon leads to unavoidable phonon scattering at the interface between MWCNTs, which limits the interfacial thermal transport (ITT) of MWCNTs [34]. It has been demonstrated that the coupling of low-frequency phonon (LFP) modes between low-dimensional nanoparticles contributes to thermal transport [35]. This enhanced is attributed to the activation of the LFP mode in nanoparticle-induced MWCNTs. It enables the redistribution of LFP modes into the C atoms of the interface, which activates resonance with the LFPs of the nanoparticles, thus enabling more heat transfer across the contact. Furthermore, one-dimensional MWCNTs have many excellent mechanical, electrical, chemical, and optical properties [36].

According to the above, the TiN and MWCNTs were firstly applied to construct the low-dimensional plasmonic nanoparticles. The optical extinction properties of low-dimensional composites were computed by the finite-difference time-domain (FDTD) method. In addition, the stable TiN/MWCNTs nanofluids were prepared by combining sanding and ultrasonic. The optical absorption and the thermal conductivity of TiN/MWCNTs hybrid nanofluids were studied. Meanwhile, the solar-thermal conversion processes of TiN/MWCNTs nanofluids were comparatively investigated by vertical mode, the experimental schematic diagram was denoted in Fig. 1. In this paper, the concept of low dimensional plasmonic nanofluids is proposed for the first time, and the mechanism of the enhancement of its photothermal conversion performance was explained from the perspective of phonon heat transfer. We believe it could provide a unique solution to broaden the spectral absorption bandwidth and enhance the photothermal conversion of nanofluids.

2. Experimental

2.1. Materials and characterization techniques

Titanium nitride (≥99.9%, 20 nm) nano-powders were purchased from Deke Daojin Science and Technology Co., Ltd (Beijing, China). Carbon nanotubes (CNTs, ≥99.4%) were supplied by Chengdu Organic Chemistry Co., Ltd. (Chengdu, China). Ethylene glycol (EG, AR) and polyvinylpyrrolidone (PVP-K30, LR) were supplied by Chron Chemical Co., Ltd (Chengdu, China).

The morphologies of nanoparticles were examined by a SU8220 scanning electron microscope (SEM, HITACHI, Japan). Raman spectra of MWCNTs and TiN/MWCNTs hybrid nanoparticles was measured by using the HORIBA Scientific LabRAM HR Evolution.

2.2. FDTD simulation of nanoparticles

Maxwell's equations were a set of fundamental equations that explain electromagnetic phenomena and they could be used to determine the interaction of electromagnetic waves with particles. The electromagnetic (EM) field distribution around the nanoparticles can be solved by combining the dielectric additional equations and suitable boundary conditions. The extinction characteristics of the material can be obtained by processing the EM field quantities. Thanks to the flexibility and accuracy of FDTD method, it could be employed to calculate the EM wave interactions between light radiation fields and arbitrary complex nanostructures [37].

In the process of numerical solution by FDTD, the construction of the model and the selection of boundary conditions were mainly considered [38]. A particular model of nano-TiN loaded on MWCNTs was shown in Fig. 2. In this model, MWCNTs had a radius of 20 nm and a length of 220 nm. Then the perfectly matched layers were selected for the simulation area to absorb almost all the incident waves. And the grid size was $1 \times 1 \times 1$ nm. EG with refractive index of 1.4318 was set as the simulated background, and the simulated light source was a total-field scattered-field (TFSF). Since the solar light was non-polarized light, it could be decomposed into two independent linearly polarized light with the same

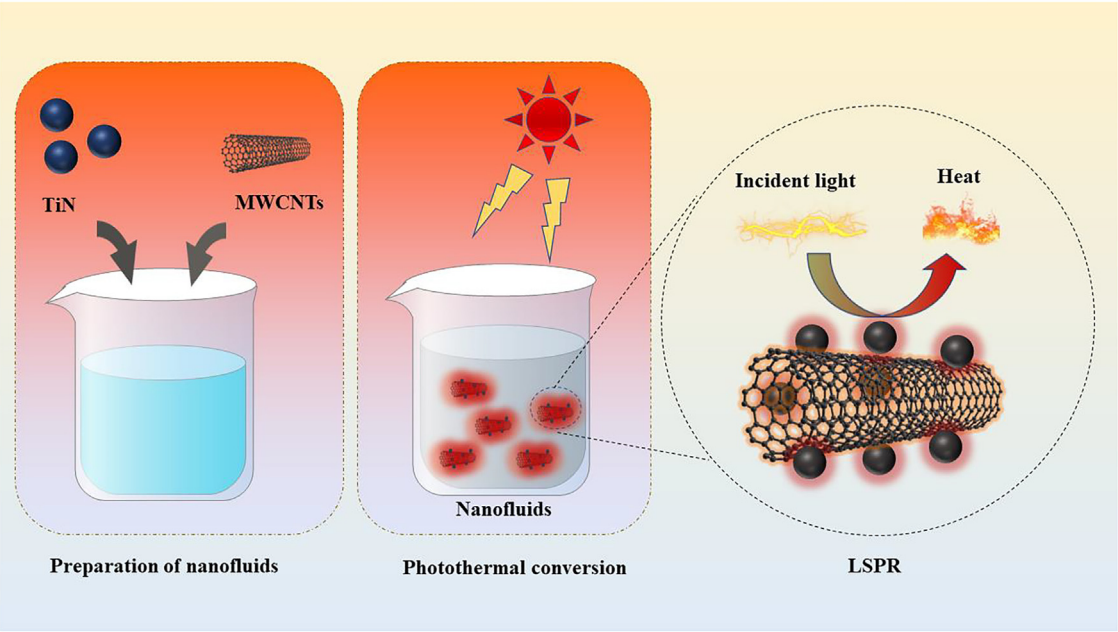

Fig. 1. Experimental schematic diagram of the TiN/MWCNTs hybrid nanofluids.

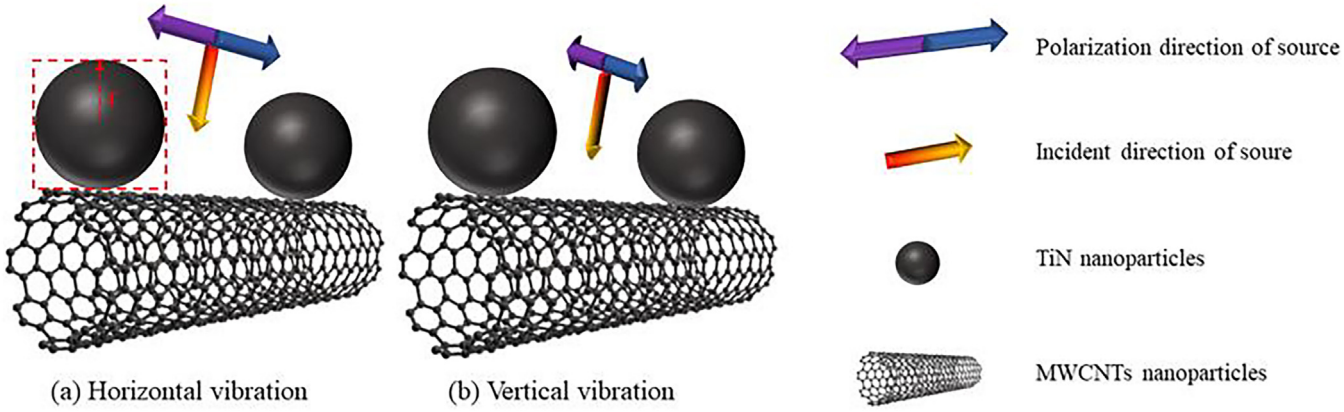

Fig. 2. The particular model of TiN/MWCNTs composites (*r* represented the radius of the TiN nanoparticles.).

intensity in vertical and horizontal directions. On this basis, the interaction of TiN/MWCNTs hybrid nanomaterials with light was explored and analyzed by FDTD.

2.3. Preparation of MWCNTs slurry

Firstly, the MWCNTs slurry with high concentration was prepared by sand milling method. The main equipment used in this step was a horizontal sand mill (NIZZOLI® 4, Puhler China) (Fig. 3). The horizontal sand mill was composed of stainless-steel stirring container, stirring medium grinding chamber and motor. The inner volume of stirring medium grinding chamber was about 450 ml. The device also had a control panel, a feeding system and a bead separator, which were not shown in the figure. The outer wall of the sanding chamber has a cavity about 3 cm thick, which was filled with EG to form a circulating cooling system during operation of the machine. The grinding media of the sand mill were solid zirconium oxide (ZrO_2) beads with diameters of 0.4–0.8 mm, and the mass of zirconium oxide beads used in this paper was 750 g. A 0.3 mm diameter separator was used at the outlet of the sanding chamber to separate the beads from the MWCNTs slurry.

In the preparation process, MWCNTs, PVP-K30 (dispersant, 2 wt.%) and the corresponding EG were first mixed in a stirring vessel at 500 rpm for 15 min. Then the cyclic grinding mode was installed to further disperse the slurry by feeding the premixed suspension into the grinding chamber, the grinder speed was 2000 rpm during grinding, and then the treated MWCNTs slurry would flow back into the stirrer vessel. Finally, a slurry of MWCNTs (4 wt.%) was obtained. Then, MWCNTs slurry was diluted to the desired concentration by simple stirring and ultrasonic.

2.4. Preparation of low-dimensional plasmonic nanofluids

To begin with, the MWCNTs nanofluids (10 ppm) were added in a beaker. Then, the TiN of different mass were added separately. The TiN/MWCNTs nanofluids with different concentrations were obtained by ultrasonic shaking for 2 h with an ultrasonic processor (Scientz Biotechnology Co., China, 500 W,20 kHz). Among them, the mass ratios of MWCNTs to TiN nanoparticles were 1:1, 1:2, 1:3, 1:4, and 1:5, which were labeled as R1, R2, R3, R4, and R5, respectively. The 10 ppm MWCNTs nanofluids was labeled as R0. In addition, the pure EG with PVP-K30 dispersant was set as a blank control group.

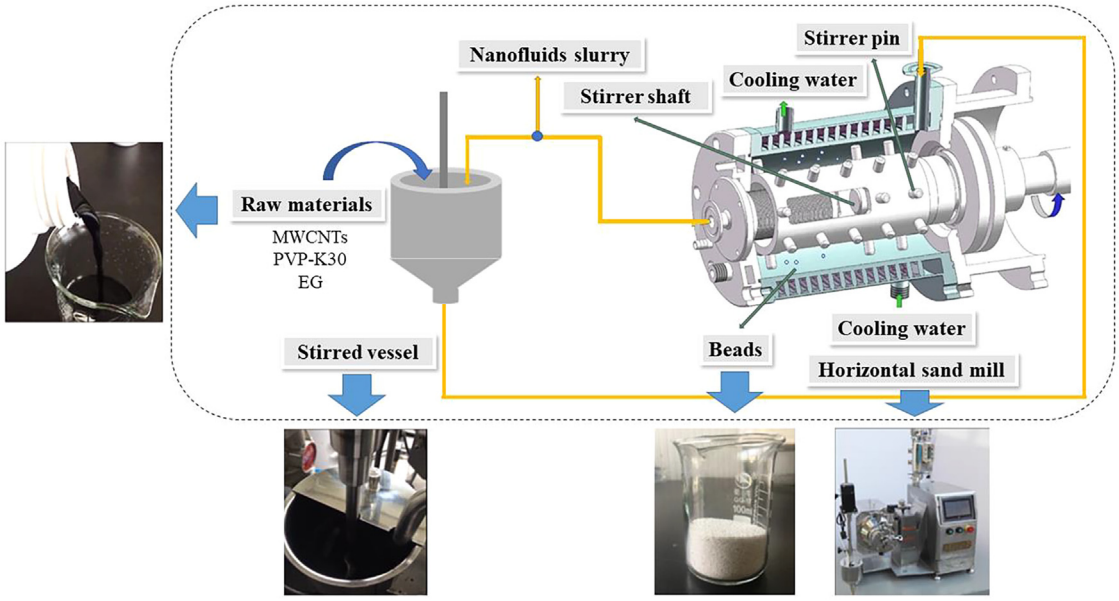

Fig. 3. The preparation process of MWCNTs slurry by sand mill.

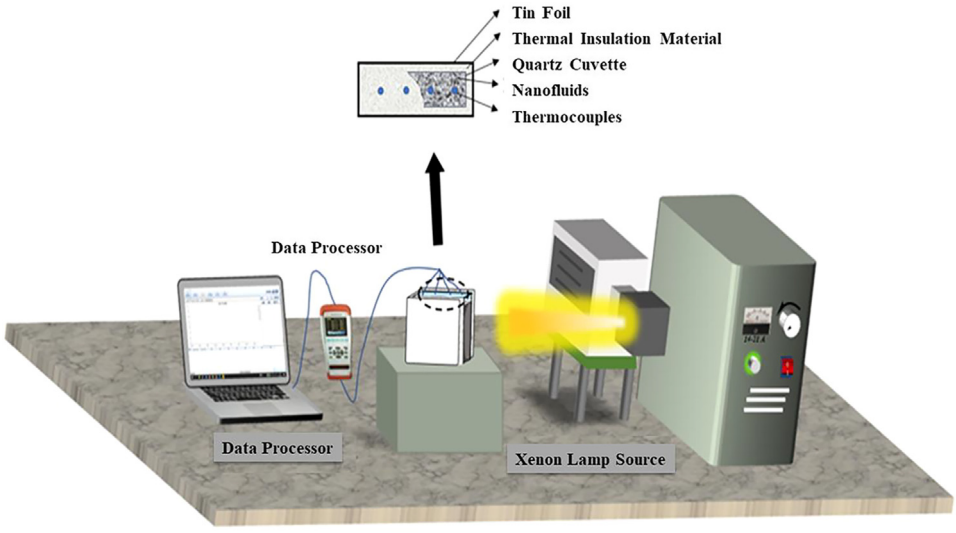

Fig. 4. Diagram of the self-made photothermal experimental device.

2.5. Optical properties

A UV–Vis spectrophotometer was employed to characterize the optical properties of nanofluids. In a typical experiment, the nanofluids sample was put into a standard quartz cuvette (optical path = 1 cm) and tested in a range of 190–1100 nm. Each sample was measured five times to reduce experimental error.

2.6. The photothermal conversion

The solar-thermal conversion properties of TiN/MWCNTs hybrid nanofluids were investigated using the self-made photothermal experimental device (Fig. 4). During the experiments, a cubic quartz cuvette (optical path = 40 mm) was used to hold the nanofluids sample in order to minimize the influence of external light, as well as reducing the heat loss. The cuvette was surrounded by the polystyrene and a tin foil as the outermost layer. Next, a CEL-HXF300 xenon lamp (China) was applied as a sunlight simulator. It was worth mentioning that the direction of incidence of the lamp source was perpendicular to the direction of gravity. The light intensity was confirmed at a certain distance using a HD2302 solar radiometer (Delta-Ohm, Italy). To fully detect the temperature variation of the nanofluids at different locations, the temperature variation of the samples under different light paths was measured by a multi-threaded thermometer (JK804, Jin Ailian Electronic Technology Co., China) (four sensors were placed evenly). And the experimentally obtained temperature data were transferred to a data processor through a recording unit (Omega-TC08), while the temperature change curve of the samples was recorded. The exposure time of the simulated xenon light source was 3000 s. The data recording interval was 10 s. The timing ended when the sample cooled naturally to room temperature.

2.7. Performance indices and error analysis

The optical absorption properties of nanomaterials could be characterized by its extinction coefficient. The scattering properties and extinction efficiency of simple spherical particles were re-

lated to the shape coefficient a and the optical constants m of the particles according to the Mie theory [39]. The a and m could be expressed as Eq. (1) and Eq. (2):

$$a = \frac{\pi D}{\lambda} \tag{1}$$

$$m = \frac{n_a + i\kappa_a}{n_b} \tag{2}$$

where D was the diameter of the particle (nm), λ denoted the wavelength of the incident light (nm), n represented the refractive index of the particles, and κ meant the light absorption index of the nanoparticle.

In particular, for spherical nanoparticles, whose particle size was significantly smaller than the wavelength of incident energy, the Mie theory can be simplified to calculate using Rayleigh scattering theory when $\alpha \ll 1$ and $\alpha \mid m-1 \mid \ll 1$. From Rayleigh scattering theory, the absorption factor (Q_a), scattering factor (Q_s), and extinction factor (Q_e) of nanoparticles were expressed by Eqs. (3), (4), and (5), respectively:

$$Q_a = 4\alpha Im\left\{\frac{m^2-1}{m^2+2}\left[1+\frac{\alpha^2}{15}\left(\frac{m^2-1}{m^2+2}\right)\frac{m^4+27m^2+38}{2m^2+3}\right]\right\} \tag{3}$$

$$Q_s = \frac{8}{3}\alpha^4 \mid \frac{m^2-1}{m^2+2}\mid^2 \tag{4}$$

$$Q_e = Q_a + Q_s \tag{5}$$

where Im was the imaginary part of the complex number. Since the volume fraction of TiN/MWCNTs nanoparticles was less than 0.6% and the particle size was less than 50 nm, it could be considered that the nanofluids were in an independent scattering state [40]. The extinction coefficient K_{np} of TiN/MWCNTs nanoparticles was calculated by Eq. (6) according to Rayleigh scattering theory:

$$K_{np} = \frac{3\varphi_v Q_e}{d_p} \tag{6}$$

where d_p was the average particle size of nanoparticles. The extinction coefficient K_b of EG can be derived by using Eq. (7) which was based on the Beer-Lambert law [20]:

$$K_b = \frac{-\ln T(\lambda)}{b} \tag{7}$$

where $T(\lambda)$ and b were the transmittance of nanofluids and optical path length (cm), respectively. In this study, the optical path length was 1 cm. The extinction coefficient of nanofluids K_{nf} could be approximated by summation the corresponding extinction coefficients of nanoparticles and EGs as Eq. (8):

$$K_{nf} = K_{np} + K_b \tag{8}$$

For further exploration of the optical properties of the hybrid nanofluids, the absorbed solar power spectrum $I_A(\lambda)$ of the nanofluids was discussed and defined according to Eq. (9) [41]:

$$I_A(\lambda) = I_{AM1.5}\left[1 - e^{-T(\lambda)b}\right] \tag{9}$$

where the wavelength range (λ) was 280–1100 nm, and $I_{AM1.5}$ was the standard solar radiation spectrum.

The solar weighted absorption fraction was derived from Eq. (10) [42]:

$$F(x) = \frac{\int I_{AM1.5}\left[1 - e^{-T(\lambda)b}\right]d\lambda}{\int I_{AM1.5}(\lambda)d\lambda} \tag{10}$$

An energy balance-based model was applied to calculate the photo-thermal conversion efficiency (PCe, η) [43], as shown in Eq. (11):

$$(mc_p + m_s c_{p,s})\frac{d\Delta T}{dt} + B\Delta T + C\Delta T^2 = \eta A I_{AM1.5}(\lambda) \tag{11}$$

where m and m_s were the mass of working fluids and the cuvette, respectively (kg); c_p and $c_{p,s}$ were the constant-pressure heat capacities, J/(kg· °C); ΔT was the temperature change at time t (s); B and C were heat dissipation coefficients; A (m^2) was radiation area. The nanofluids concentration in this experiment was relatively low, so c_p could be approximated as the constant-pressure heat capacity of EG. The values of B and C could be confirmed from the energy balance at the end of the radiation, as indicated in Eqs. (12) and (13):

$$(mc_p + m_s c_{p,s})\frac{d\Delta T}{dt} + B\Delta T + C\Delta T^2 = 0 \tag{12}$$

$$\Delta T^{-1} = D \cdot \exp\left(\frac{Bt}{mc_p + m_s c_{p,s}}\right) - \frac{C}{B} \tag{13}$$

where B, C and D could be obtained by fitting the data points of the cooling process.

When the temperature of the nanofluids reached equilibrium, η could be calculated by Eqs. (14) and (15):

$$B\Delta T + C\Delta T^2 = \eta A I_{AM1.5}(\lambda) \tag{14}$$

$$\eta = \frac{B\Delta T + C\Delta T^2}{A I_{AM1.5}(\lambda)} \tag{15}$$

The experimental errors in the photothermal conversion experiments were caused by different measurement errors, which included the relative errors in the weight of the nanofluids (m), the temperature of the thermocouples (T), the optical depth (l) and the radiation intensity (I). Thus, the experimental uncertainty (E_η) [44] could be expressed as Eq. (16):

$$E_\eta = \sqrt{\left(\frac{\delta m}{m}\right)^2 + \left(\frac{\delta T_i}{T_i}\right)^2 + \left(\frac{\delta T_f}{T_f}\right)^2 + \left(\frac{\delta l}{l}\right)^2 + \left(\frac{\delta G}{G}\right)^2} \tag{16}$$

The weight of nanofluids was measured by using an analytical balance (accuracy ±0.0001 g), the nanofluids temperature was measured by a thermocouple meter (accuracy ±0.1 °C), the optical range was measured by a vernier caliper (accuracy ±0.02 mm), and the spectral irradiance was measured by a solar radiometer (accuracy ±2%). The calculation by substituting the experimental data showed that the maximum relative error of the photothermal PCe measured in this experiment was 3.13%.

3. Results and discussion

3.1. Characteristics

The morphologies of different nanoparticles were displayed in Fig. 5. The nano-TiN were spherical with a diameter of about 20 nm and some agglomeration existed (Fig. 5(a)). MWCNTs were long straight cylinders with a tube diameter of about 10 nm (Fig. 5(b)). The SEM images of TiN/MWCNTs hybrid nanoparticles was demonstrated in Fig. 5(c). The above results indicated that TiN nanoparticles were distributed on the surface of MWCNTs. Moreover, the hybrid TiN/MWCNTs nanofluids was prepared successfully and they processed good stability (Support Information Section S1).

3.2. FDTD results

The accuracy and validity of the simulations were verified by comparing the simulation results of the real part (Re) and imaginary part (I_m) of the dielectric constants of the TiN nanoparticles and MWCNTs models with the results in the literature (Supporting Information Section S2.1). Moreover, the calculation results of the FDTD method agreed well with the Mie theory values, and the

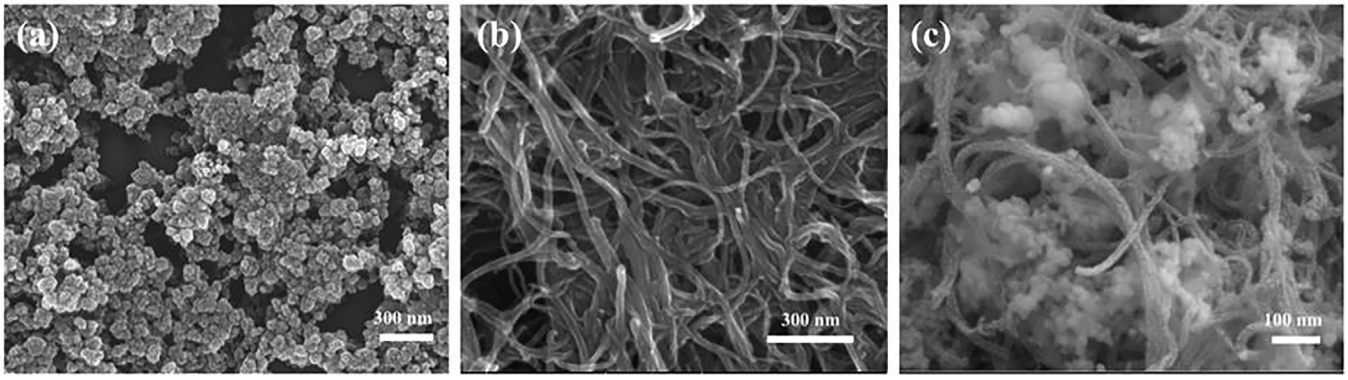

Fig. 5. SEM pictures of nanoparticles: (a) TiN, (b) MWCNTs, (c) TiN/MWCNTs.

FDTD model exhibited excellent accuracy (Supporting Information S2.2, Fig. S4). In summary, the simulated values of the model established in this study provided some guidance for the later experiments, and the credibility of the simulation results was achieved.

The results of the absorption cross-sectional area and electric field distribution for two different incidence modes were presented in Fig. 6. The radius (r) of TiN nanoparticles was 20 nm. When the horizontal vibration mode (HV mode) was conducted on the MWCNTs particles, based on Fig. 6(a), the resonance peaks of the double TiN nanoparticles were observed to be blue-shifted with the increase of the TiN nanoparticle spacing. In addition, the absorption intensity weakened and gradually resembled the shape of the resonance peaks of the single nanoparticles with the same resonance peak position. When the number of nano-TiN changes from 1 to 2, the maximum increase of absorption cross section was 44.4% at δ =1 nm, which proved that the LSPR resonance effect generated by multiple nanoparticles could enhance the absorption of the light. In particular, when the particle spacing δ decreased from 50 to 1 nm, the horizontal vibrational incident light skewed the TiN nanoparticle resonance peak position by 56 nm. On the contrary, when the incident light vibrates vertically (the direction of the incident polarized light was perpendicular to the direction of the center axis of MWCNTs) (Fig. 6(c)), the distance of TiN nanoparticles increased, their resonance peaks were red-shifted, and the resonance intensity was slightly enhanced, but the difference with the intensity of single TiN nanoparticles was not significant. The incident light shifted the resonance peak position of TiN nanoparticles by 5 nm under vertical vibration. When the number of TiN nanoparticles was 2 and δ was 1 nm, the absorption cross section was 7.7% larger than that of the single TiN particle. It indicated that the incident light of perpendicular resonance had an inhibitory effect on the internal electric field resonance of the particles, but the effect was not obvious.

Simultaneously, the electric field intensity distributions of the two-particle system in the surrounding area of the incident magnetic field horizontal vibration (Fig. 6(b)) and the vertical vibration mode (VV mode) (Fig. 6(d)) were depicted. The electric field of the nanoparticle interaction was significantly enhanced for the incident horizontally vibrating linearly polarized light with a spacing of 1 nm, which was about three times of the electric field intensity around the single particle. It was attributed to the resonance between TiN nanoparticles, which enhanced the absorption ability of electromagnetic waves and effectively increased the absorption cross section (Fig. 6(b)). The interaction between the two nanoparticles was quite weak when the spacing was 50 nm, and the electric field distribution around the two particles was similar to that of the isolated nanoparticles. The electric field intensity inside the gap of particles with the same particle spacing and incident vertical vibrational line polarization light did not change due to the suppression of the resonant electric field inside the particles. Therefore, during the photothermal conversion of nanoparticles, the incident light of horizontal vibration mainly excited the nanoparticles to produce heat. Moreover, the resonance enhancement and peak shift of the HV mode were more prominent than those of the VV mode. It was indicated that the HV mode plays a major role in influencing the nanostructure under the superposition of the two modes. In addition, we also explored the influence of TiN nanoparticles percentage on the light absorption performance (Section S2.3). The results indicated that the increase of particle number and the nanoparticles in a homogeneous electric field environment were beneficial to the light absorption of the multi-particle system. Similarly, the effect of TiN nanoparticle size on the light absorption performance was studied (Section S2.4). The analysis results showed that increasing the size of nanoparticles in a certain range can effectively enhance the PCe. Thus, the intensity and width of spectral absorption could be enhanced by using low-dimensional plasmonic nanostructure.

3.3. Optical properties of nanofluids

The excellent light absorption properties of nanofluids is the prerequisite for their high PCe. The stronger the absorption of incident light by the nanofluids, the more sufficient energy was available for photothermal conversion. In Section 3.2, the LSPR effect of the hybrid nanoparticles was verified theoretically by FDTD simulations. Next, the optical absorption properties of the hybrid nanofluids were evaluated from an experimental point of view. The UV–vis spectra of TiN/MWCNTs nanofluids were shown in Fig. 7(a). Overall, the TiN/MWCNTs hybrid nanofluids could effectively reduce the EG transmission rate by a maximum of 80.88%. In addition, the absorption intensity was increased with the weight ratio from R0 to R5, which indicated that the solar absorption of EG could be significantly improved by the addition of nanoparticles. It was similar to the conclusion in FDTD. Specifically, the spectral transmittance of R0 nanofluids was about 50% in the range of 400–1100 nm, which was about half of that of EG. And the spectral transmittance of nanofluids gradually decreased as the concentration of TiN nanoparticles increased. The average spectral transmittance of R4 nanofluids was as low as 2.4%, and the average spectral transmittance of R5 nanofluids was only 0.8%. The reason could be attributed that LSPR of TiN nanoparticles enhanced and broadened the absorption ability of incident light by the fluid. The transmittance indicated that the TiN/MWCNTs hybrid nanofluids could trap solar radiation and could positively affect the PCe.

The curves in Fig. 7(b) represented the theoretical absorption of the spectral irradiance with the TiN/MWCNTs nanofluids, and the area under the curves expressed the solar energy absorbed by the nanofluids (calculated by Eq. (9)). It is another important factor in

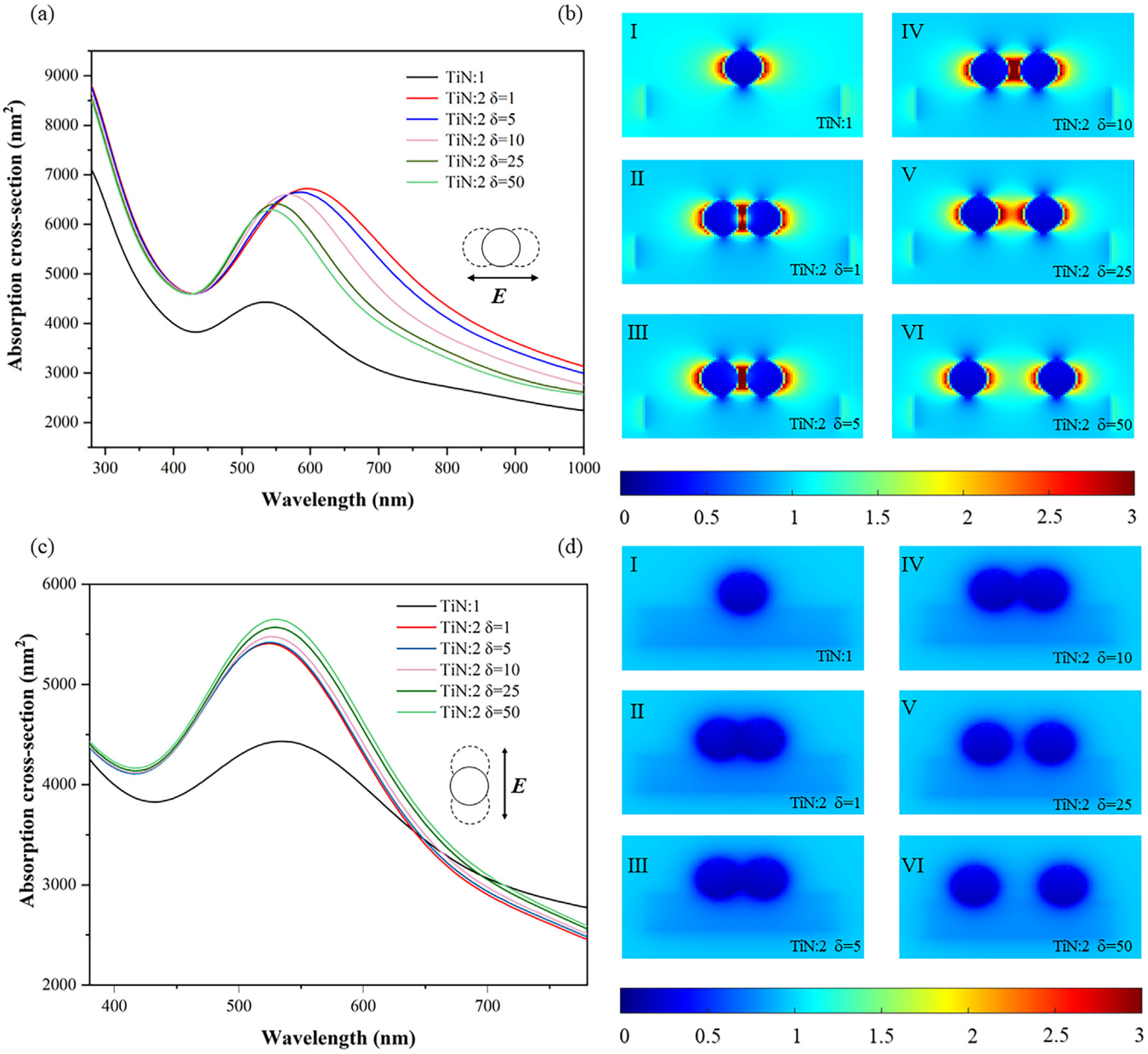

Fig. 6. Numerical simulation results of FDTD for the TiN/MWCNTs dual nanoparticle system. (a) and (b): Numerical simulation results in HV mode; (c) and (d): in VV mode.

evaluating the optical properties of nanofluids. It was obvious that the absorption of EG was incomplete and could only reach about 10%. Similarly, the absorption of MWCNTs nanofluids (R0) was only 55%. In contrast, R1 nanofluids (10 ppm) could already theoretically absorb 75% of solar energy, and the curve of R5 nanofluids almost coincided with the solar radiation spectrum curve. This indicated that the LSPR of the nano-TiN improved the light absorption capacity of the whole system. In addition, it was noteworthy that the light-trapping ability of the nanofluids was influenced by the concentration of TiN nanoparticles significantly. However, when the concentration reached a certain level, the effective capture of solar energy by nanofluids would encounter a bottle neck. In other words, R4 and R5 nanofluids can absorb almost all the solar radiation. Thus, it was essential to study the optimal combination of nanomaterial properties and concentrations for the solar energy absorption processes.

Furthermore, the selection of the optimal fluid depth in solar-thermal conversion was an unavoidable issue. The use of nanofluids as light absorbing media for collectors could reduce the fluid depth effectively. However, if the fluid depth was small, it would not be able to convert and store enough incident energy [45]. Therefore, choosing the right fluid depth was very important. A plot of the energy weighted absorption fraction versus optical penetration distance for TiN/MWCNTs nanofluids was illustrated in Fig. 7(c) (calculated by Eq. (10)). The solar energy weighted absorption fraction of the nanofluids could be seen to increase with the penetration distance. At the same time, the nanoparticle concentration had a significant effect with respect to the solar energy weighted absorption fraction. Particularly, the energy absorption fraction of R0 nanofluids was 55.1% (optical penetration depth = 1 cm), which was 26.6% lower than that of 75.1% for R1 nanofluids. This demonstrated that TiN nanoparticles could enhance the light absorption properties of TiN/MWCNTs nanofluids. In addition, the solar energy weighted absorption fraction of R5 was already close to 100% when the penetration distance was 1 cm. This meant that only extremely thin nanofluids layers were

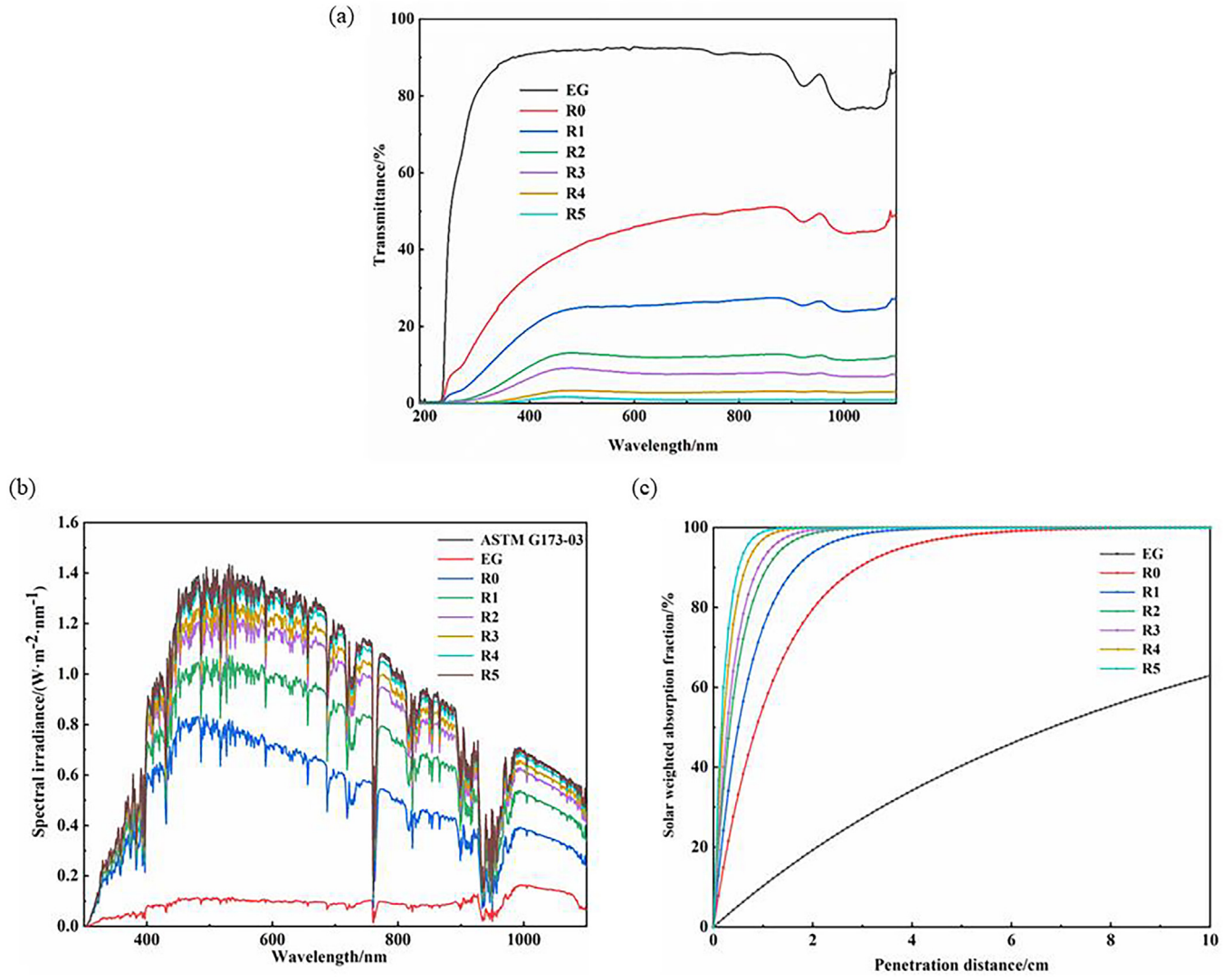

Fig. 7. (a)Transmittance of TiN/MWCNTs nanofluids. (b) Spectral irradiance of the nanofluids with different nano-TiN concentration (penetration distance = 1 cm). (c) The solar weighted absorption fraction of different nanofluids.

required to achieve efficient solar energy absorption, which was highly beneficial for its photothermal conversion process.

3.4. Thermal conductivity of nanofluids

The heat transfer characteristics of nanofluids would directly affect its photothermal conversion characteristics. Nanofluids with high thermal conductivity are able to transfer heat to the low temperature nanofluids in a timely manner. This could avoid the enhanced heat radiation to the environment due to the high temperature of the nanofluids surface. Therefore, nanofluids with high thermal conductivity can reduce heat loss and hence increase PCe.

LFP is important for carrying thermal energy [46]. Raman spectroscopy was used to study the changes in phonon vibration modes of MWCNTs after decorated with TiN nanoparticles. By applying 514 nm excitation, it was found that nano-TiN has a similar effect as nano-Au to blueshift the G-band and second-order G′-band of MWCNTs (Fig. 8) [35]. Blueshift is an equivalent *p*-type doping effect which can induce the transformation of some sp^2 (graphite-like) C—C bonds to some weak sp^3 (diamond-like) bonds without affecting the surface structure of MWCNTs. The decrease in C—C bonds strength can induce a decrease in curvature energy owing to the $sp^2 \rightarrow sp^3$ transition. This caused a decrease in the frequency of the low-frequency breathing phonon mode [47]. Therefore, the Raman shift offered evidence of the contribution of TiN nanoparticles to the induction of LFP vibrations of C atoms in MWCNTs.

To investigate the effect of LFP mode on the heat transfer process, the thermal conductivity of the TiN/MWCNTs nanofluids was measured (Section S3). The results indicated that the addition of both MWCNTs and nano-TiN could effectively improve the performance of EG in terms of thermal conductivity. In Fig. 9, the thermal conductivity of hybrid nanofluids was positively correlated with both temperature and concentration. At the room temperature, the thermal conductivity of R0 was increased by 3.7% compared to EG. Furthermore, the thermal conductivity of R5 was increased by 10.9% compared with the R0 nanofluids.

In addition, the thermal conductivity of nanofluids formed by the continued addition of nano-TiN to the MWCNTs nanofluids was further improved (Fig.S8). This is due to the LFP resonance effect between TiN nanoparticles and MWCNTs. TiN containing abundant LFP modes can induce low-frequency vibrations of C atoms in MWCNTs to excite more long-wave phonons (Fig. 10). The number of LFPs in the interfacial C atoms gradually increases with the increase of the number of participating TiN nanoparticles. A large number of LFP modes can be generated on nano TiN surface, which may induce LFP vibrations in MWCNTs to benefit ITT

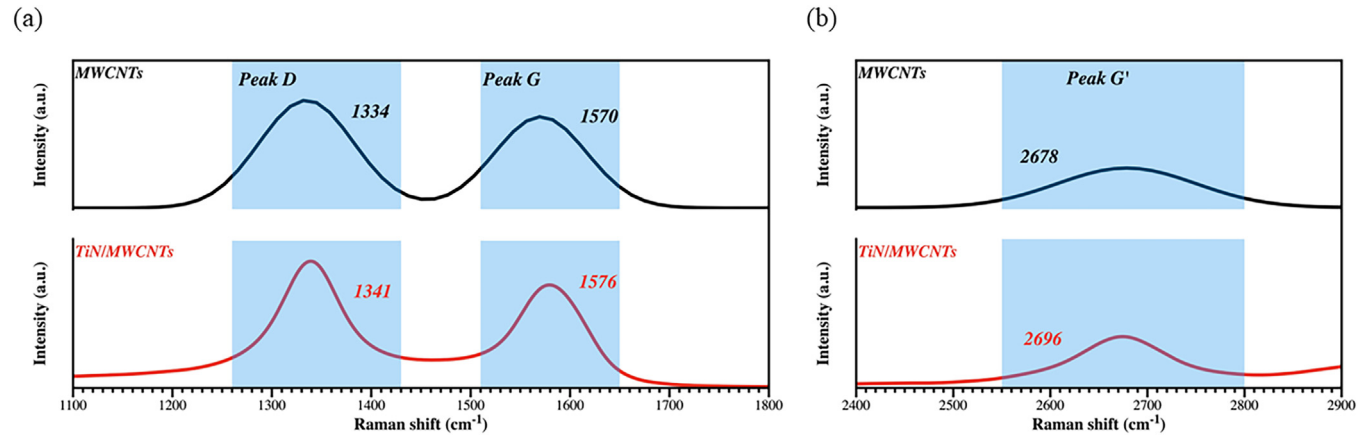

Fig. 8. Comparison of the fitted Raman spectra of different MWCNTs (excitation energy of 514 nm). (a) TiN decoration leads to a shift of 7- and 6- cm^{-1} in the D and G peaks at this excitation energy. (b) The G′ peak has a significant shift (18- cm^{-1}).

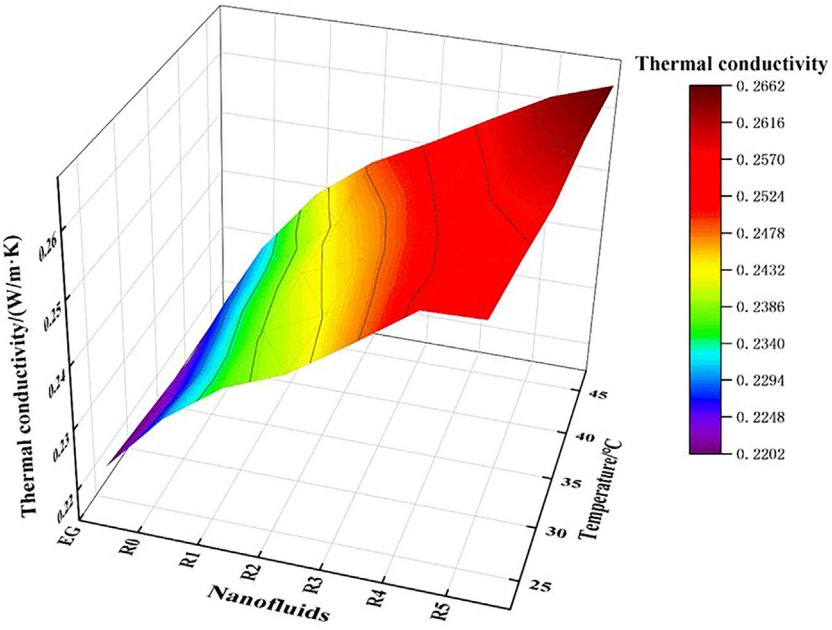

Fig. 9. Thermal conductivity of different nanofluids (R0~R5).

[48,49].Since the LFP mode carries the dominant lattice vibration energy [50], the heat conduction of the MWCNTs-TiN-MWCNTs system will be enhanced accordingly. Hence, the thermal conductivity of TiN/MWCNTs hybrid nanofluids was improved, which could be more conducive to rapid heat transfer in the photothermal conversion process.

3.5. Photothermal conversion efficiency

A special coupled flow and solar thermal model was employed in this study (Fig. 11), which used solar radiation perpendicular to the gravity direction (Fig. 11(b)). In general mode (Fig. 11(a)), the energy conversion process in the lower nanofluids layer was depended on the heat conduction in the upper layer. Also, since the highest temperature of the nanofluids occurred on the upper absorbing surface, it might cause higher heat loss to the environment. To a certain extent, the acceleration of the motion of nanoparticles along the direction of gravity caused by heat conduction intensified the accumulation of nanoparticles at the bottom. Through the lateral solar radiation, the nanofluids would move upward after heating due to density drop and volume expansion. Afterwards, it replenished by a cooler fluid along the other side to form a working cycle. Compared with the general model, this internal heat cycle accelerated the heat transfer of the nanofluids and reduced the temperature difference. In addition, it promoted the thermal motion of nano materials, thus reducing the movement of nanoparticles toward the bottom and keeping the particles inside the absorber from accumulating.

The original temperature rise curves of TiN/MWCNTs nanofluids were presented in Fig. S 10. The energy absorption of TiN/MWCNTs nanofluids after 3000 s of illumination was exhibited in Fig. 12(a). In total, the light source provided 1560 J of energy during this time, while the EG could only uptake 770 J of energy. After adding MWCNTs, the energy absorption value of R0 increased to 864 J, which was 12.21% higher compared to EG. After adding different concentrations of nano-TiN, it was obvious that the energy absorption values of the hybrid nanofluids followed a trend of increasing and then decreasing with the concentration. The energy absorption of R4 nanofluids to the simulated light source reached the maximum value of 1192 J, which increased by 37.96% compared with R0. The results again demonstrated that TiN/MWCNTs could trap solar radiation more efficiently and convert it into thermal

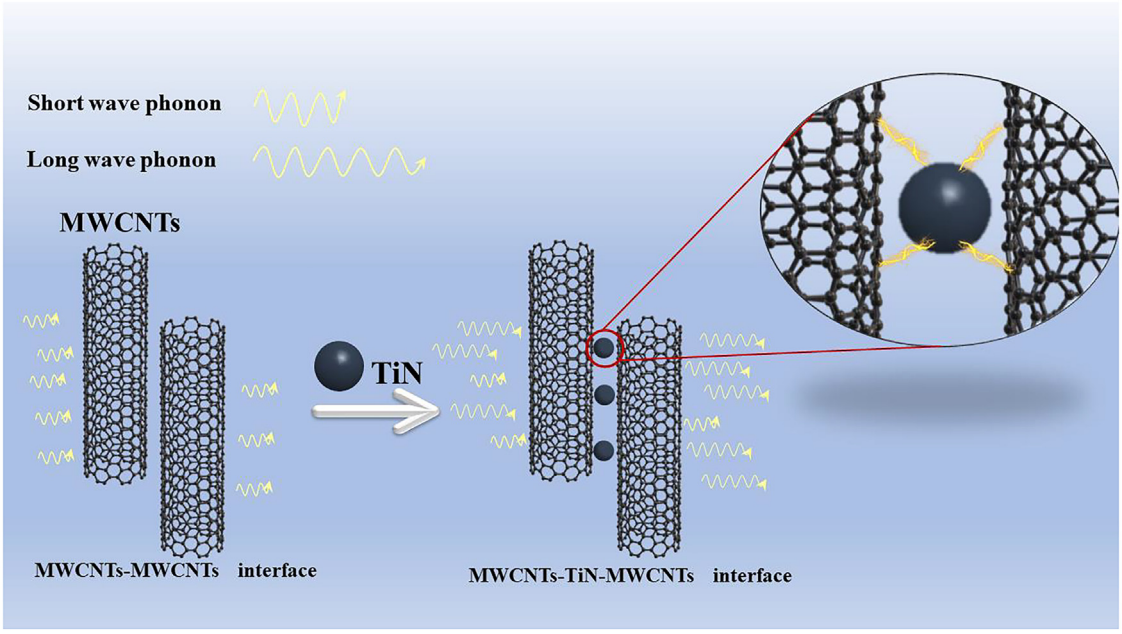

Fig. 10. Schematic diagram of LFP mode with one-dimensional MWCNTs and zero-dimensional TiN nanoparticles.

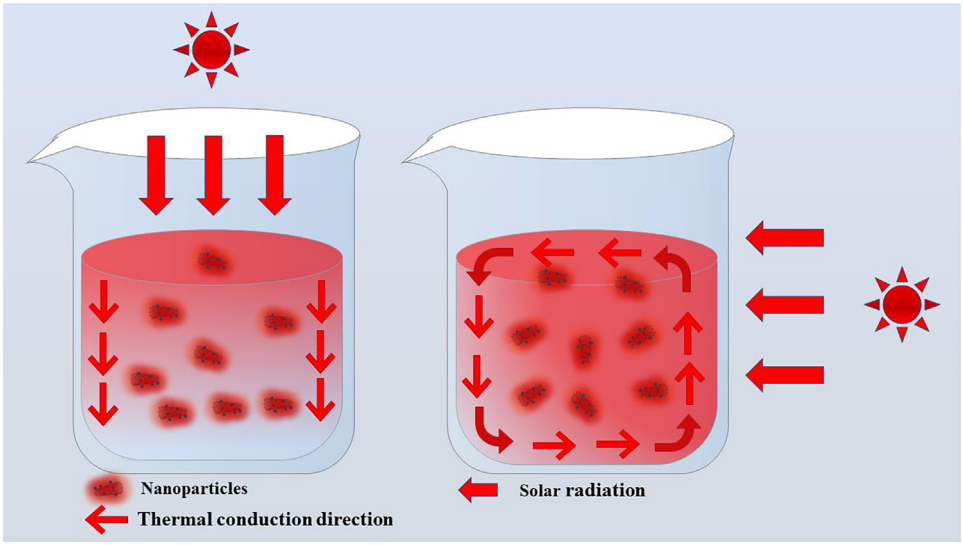

Fig. 11. Photothermal coupling models of (a) parallel mode or (b) vertical mode.

energy owing to its LSPR effect and excellent phonon transport capability.

In this experiment, an equation model considering the heat loss of nanofluids was used (Eq. (15)). The PCe and temperature rise of TiN/MWCNTs nanofluids were plotted against nanofluids concentration in Fig. 12(b). It was shown from the figure that the regularity of the PCe was consistent with the temperature rise, and both showed an increasing and then decreasing trend with the increase of nanofluids concentration. Specifically, the PCe of R0 was 55.4% with the addition of MWCNTs, which was increased by 6.1% relative to EG. Meanwhile, with the introduction of nano-TiN, the efficiency of R1 reached 68.1%, while with the increasing content of TiN, the efficiency of R4 was enhanced by 54% compared to the base fluids. It proved the excellent PCe of TiN/MWCNTs hybrid nanofluids. Two main reasons can be attributed to this phenomenon. (1) nano-TiN possessed LSPR effects, so its combination with MWCNTs could improve light absorption. (2) The LFPs resonance of zero-dimensional TiN nanomaterials with MWCNTs facilitates the interfacial heat transport and improves the thermal conductivity. Similar to the energy absorption, the peak efficiency appeared at R4 nanofluids, which was 76.4%. The efficiency of R5 nanofluids was slightly lower than that of R4 at 74.2%. The reason for this might be that the high concentration of nanofluids had certain surface absorption properties. This meant that the heat transformed by the nanofluids was mainly concentrated at the surface of the fluid, and the temperature difference with the external environment as well as the deep fluid increased. Eventually, it leads to increased heat loss. Thus, the PCe eventually trended downward.

All in all, the above findings in the photothermal part confirmed the high PCe of TiN/MWCNTs nanofluids. And the R4 nanofluids could almost completely absorb the sunlight and achieved a PCe of 76.4%. In other words, further increasing the concentration of nanoparticles would have no significant effect on the improvement of the PCe. In specific application situation, the particular con-

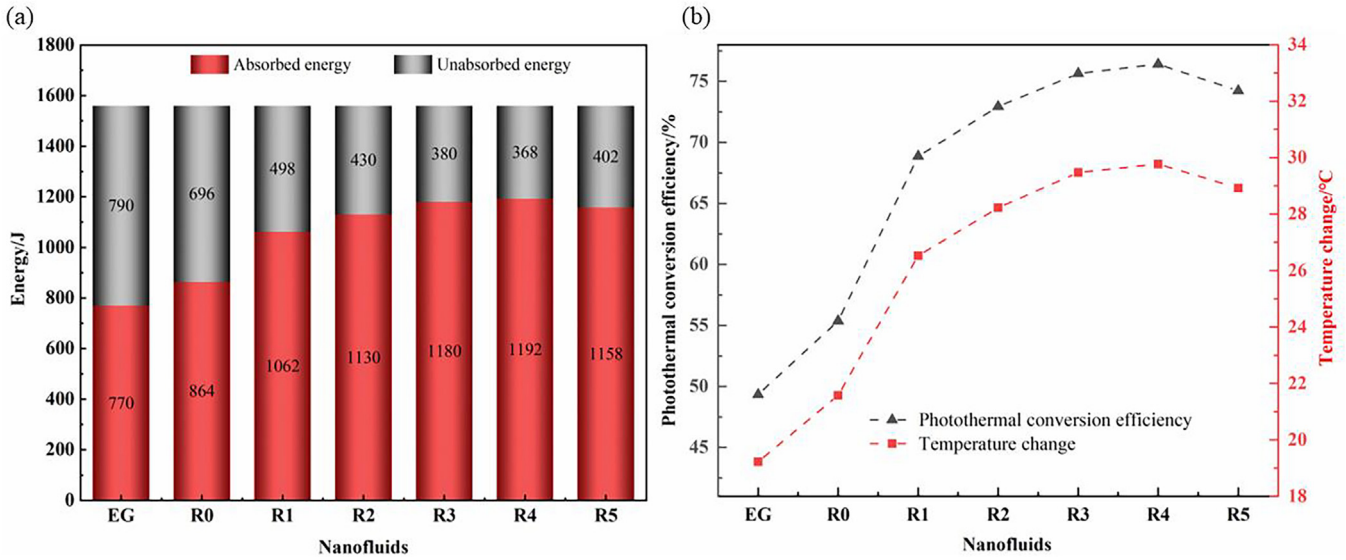

Fig. 12. (a) Energy absorption and (b) comparison of temperature rise and photothermal conversion efficiency (PCe) of TiN/MWCNTs hybrid nanofluids.

centration should be carefully considered by determining the efficiency, fluid depth and preparation cost.

4. Conclusions

In this study, the low-dimensional plasmonic TiN/MWCNTs nanofluids were prepared. And the mechanism of the enhancement of its photothermal conversion performance was explained from the perspective of phonon heat transfer.

(1) FDTD numerical simulations disclosed the coupling effect among TiN nanoparticles and MWCNTs. Experiments demonstrated that the light absorption performance of the low-dimensional plasmonic nanofluids was enhanced because of the LSPR effect of TiN nanoparticles. And the maximum absorption fraction of TiN/MWCNTs hybrid nanofluids can reach 98% (R5).
(2) The addition of both MWCNTs and TiN nanoparticles could effectively improve the thermal conductivity of EG. And the thermal conductivity of the nanofluids formed by the continued addition of TiN nanoparticles to MWCNTs nanofluids was further improved. This is owed to the LFP resonance effect between TiN particles and MWCNTs.
(3) Owing to the unique LSPR effect and LFP mode of TiN/MWCNTs nanofluids, the PCe of nanofluids showed a parabolic pattern with increasing concentration. And the maximum PCe of low-dimensional plasmonic nanofluids reached 74.2% (40 ppm).

Declaration of competing interest

We declare that we have no financial and personal relationships with other people or organizations that can inappropriately influence our work, there is no professional or other personal interest of any nature or kind in any product, service and/or company that could be construed as influencing the position presented in, or the review of, the manuscript entitled, "**The mechanism of enhanced photothermal conversion of low-dimensional plasmonic nanofluids with LFPs resonance**".

CRediT authorship contribution statement

Rui Yang: Investigation, Software, Visualization, Writing – original draft. **Xiaoke Li:** Supervision, Project administration, Writing – review & editing. **Fei Yin:** Conceptualization, Funding acquisition. **Jinwen Shi:** Methodology, Funding acquisition, Validation. **Dengwei Jing:** Resources, Data curation, Writing – review & editing.

Data availability

No data was used for the research described in the article.

Acknowledgments

The authors would like to acknowledge the financial support by Sichuan Science and Technology Program (2022NSFSC0224 and 2022NSFSC0249) and National Natural Science Foundation of China (52276213). The authors would like to thank Shiyanjia Lab (www.shiyanjia.com) for the SEM and Raman analysis.

Supplementary materials

Supplementary material associated with this article can be found, in the online version, at doi:10.1016/j.ijheatmasstransfer.2023.124056.

References

[1] N.L. Panwar, S.C. Kaushik, S. Kothari, Role of renewable energy sources in environmental protection: a review, Renew. Sustain. Energy Rev. 15 (3) (2011) 1513–1524.
[2] T. Jia, Y. Dai, R. Wang, Refining energy sources in winemaking industry by using solar energy as alternatives for fossil fuels: a review and perspective, Renew. Sustain. Energy Rev. 88 (2018) 278–296.
[3] W. Yuan, J. Ji, Z. Li, F. Zhou, X. Ren, X. Zhao, S. Liu, Comparison study of the performance of two kinds of photovoltaic/thermal(PV/T) systems and a PV module at high ambient temperature, Energy 148 (2018) 1153–1161.
[4] B.Izani Vincenzo, Credi Alberto, Venturi Margherita, Photochemical Conversion of Solar Energy, Chemsuschem, 2008.
[5] Z. Qian, W. Xu, X. Wang, Carbon nanocomposites with high photothermal conversion efficiency, Sci. China Mater. (2018) 1–10.
[6] J. Li, X. Zhang, B. Xu, M. Yuan, Nanofluid research and applications: a review, Int. Commun. Heat Mass Transf. 127 (1) (2021) 105543.
[7] H. Chen, L. Zhang, P. Jie, Y. Xiong, P. Xu, H. Zhai, Performance study of heat-pipe solar photovoltaic/thermal heat pump system, Appl. Energy 190 (15) (2017) 960–980 MAR..
[8] C. Asaa, B. Fae, A. Hbb, B. Zmo, Improving the trays solar still performance using reflectors and phase change material with nanoparticles, J. Energy Storage, 31.
[9] S. Choi, J.A. Eastman, Enhancing thermal conductivity of fluids with nanoparticles, Asme Fed. 231 (1) (1995) 99–105.
[10] A. Rafiei, R. Loni, S.B. Mahadzir, G. Najafi, S. Pavlovic, E. Bellos, Solar desalination system with a focal point concentrator using different nanofluids, Appl. Therm. Eng. 174 (2020).

[11] Z. Said, M. Gupta, H. Hegab, N. Arora, A.M. Khan, M. Jamil, E. Bellos, A comprehensive review on minimum quantity lubrication (MQL) in machining processes using nano-cutting fluids, Int. J. Adv. Manuf. Technol. 105 (5–6) (2019) 2057–2086.
[12] C. Zhang, C. Shen, Y. Zhang, K. Zheng, J. Pu, X. Zhao, X. Ma, Experimental study of indoor light/thermal environment with spectrally selective windows using ATO nanofluids in winter, Energy Build. 278 (2023) 112597.
[13] Z. Said, S.M.A. Rahman, M. El Haj Assad, A.H. Alami, Heat transfer enhancement and life cycle analysis of a Shell-and-Tube Heat Exchanger using stable CuO/water nanofluid, Sustain. Energy Technol. Assess. 31 (2019) 306–317.
[14] Z. Said, M.H. Sajid, R. Saidur, G.A. Mahdiraji, N.A. Rahim, Evaluating the optical properties of TiO2 Nanofluid for a direct absorption solar collector, Numer. Heat Transf., Part A: Appl. 67 (9) (2015) 1010–1027.
[15] P. Kanti, K.V. Sharma, K.M. Yashawantha, M. Jamei, Z. Said, Properties of water-based fly ash-copper hybrid nanofluid for solar energy applications: optimization of the experimental data using RBF model, Solar Energy Mater. Solar Cells (2022) 234.
[16] C. Boerigter, R. Campana, M. Morabito, S. Linic, Evidence and implications of direct charge excitation as the dominant mechanism in plasmon-mediated photocatalysis, Nat. Commun. 7 (2016).
[17] S. Marquez, E. Morales-Narvaez, Lab Nacl micro nanofluidica, nanoplasmonics in paper-based analytical devices, Front. Bioeng. Biotechnol. 7 (2019).
[18] J. Wen, X. Li, H. Zhang, M. Chen, X. Wu, Enhancement of solar absorption performance using TiN@SiCw plasmonic nanofluids for effective photo-thermal conversion: numerical and experimental investigation, Renew. Energy (2022).
[19] E.P. Bandarra Filho, O.S.H. Mendoza, C.L.L. Beicker, A. Menezes, D. Wen, Experimental investigation of a silver nanoparticle-based direct absorption solar thermal system, Energy Conver. Manag. 84 (2014) 261–267.
[20] M. Chen, Y. He, J. Huang, J. Zhu, Investigation into Au nanofluids for solar photothermal conversion, Int. J. Heat Mass Transf. 108 (2017) 1894–1900.
[21] A.R. Mallah, S.N. Kazi, M.N.M. Zubir, A. Badarudin, Blended morphologies of plasmonic nanofluids for direct absorption applications, Appl. Energy (2018) 229.
[22] Y. Zhou, A. Huang, H. Luo, P. Jin, Localized surface plasmon resonance induced excellent solar-shielding ability for TiN nanoparticles-based hybrid polymer optical foils with high transparency, J. Alloys Compound. (2018).
[23] V. Gururaj Naik, Jongbum Kim, Alexandra Boltasseva, Oxides and nitrides as alternative plasmonic materials in the optical range [Invited], Opt. Mater. Express (2011).
[24] L. Wang, G. Zhu, M. Wang, W. Yu, J. Zeng, X. Yu, H. Xie, Q. Li, Dual plasmonic Au/TiN nanofluids for efficient solar photothermal conversion, Solar Energy 184 (2019) 240–248 MAY.
[25] J. Wen, X. Li, W. Chen, J. Liu, Systematical investigation on the solar-thermal conversion performance of TiN plasmonic nanofluids for the direct absorption solar collectors, Colloid. Surf. A (2021) 624.
[26] J. Sarkar, P. Ghosh, A. Adil, A review on hybrid nanofluids: recent research, development and applications, Renew. Sustain. Energy Rev. 43 (2015) 164–177.
[27] N.A.C. Sidik, I.M. Adamu, M.M. Jamil, G.H.R. Kefayati, R. Mamat, G. Najafi, Recent progress on hybrid nanofluids in heat transfer applications: a comprehensive review, Int. Commun. Heat Mass Transf., 78 (2016) 68–79.
[28] Y. Xuan, H. Duan, Research on photo-thermal properties of plasmonic nanofluid, Scientia Sinica Technologica 44 (8) (2014) 833–838.
[29] R. Lee, J.B. Kim, C. Qin, H. Lee, B.J. Lee, G.Y. Jung, Synthesis of Therminol-based plasmonic nanofluids with core/shell nanoparticles and characterization of their absorption/scattering coefficients, Solar Energy Mater. Solar Cells 209 (2020) 110442.
[30] G. Zhu, L. Wang, N. Bing, H. Xie, W. Yu, Enhancement of photothermal conversion performance using nanofluids based on bimetallic Ag-Au alloys in nitrogen-doped graphitic polyhedrons, Energy 183 (2019) 747–755.
[31] L. Wang, G. Zhu, M. Wang, W. Yu, J. Zeng, X. Yu, H. Xie, Q. Li, Dual plasmonic Au/TiN nanofluids for efficient solar photothermal conversion, Solar Energy 184 (2019) 240–248.
[32] P. Wang, R. Xiang, S. Maruyama, Chapter two - thermal conductivity of carbon nanotubes and assemblies, in: E.M. Sparrow, J.P. Abraham, J.M. Gorman (Eds.), Advances in Heat Transfer, Elsevier, 2018, pp. 43–122.
[33] N. Mehra, L. Mu, T. Ji, X. Yang, J. Kong, J. Gu, J. Zhu, Thermal transport in polymeric materials and across composite interfaces, Appl. Mater. Today 12 (2018) 92–130.
[34] W.J. Evans, M. Shen, P. Keblinski, Inter-tube thermal conductance in carbon nanotubes arrays and bundles: effects of contact area and pressure, Appl. Phys. Lett. 100 (26) (2012).
[35] L. Qiu, H. Zou, X. Wang, Y. Feng, X. Zhang, J. Zhao, X. Zhang, Q. Li, Enhancing the interfacial interaction of carbon nanotubes fibers by Au nanoparticles with improved performance of the electrical and thermal conductivity, Carbon N Y 141 (2019) 497–505.
[36] J. Qu, M. Tian, X. Han, R. Zhang, Q. Wang, Photo-thermal conversion characteristics of MWCNT-H2O nanofluids for direct solar thermal energy absorption applications, Appl. Therm. Eng. 124 (2017) 486–493.
[37] A.R. Mallah, M.N. Mohd Zubir, O.A. Alawi, K.M. Salim Newaz, A.B. Mohamad Badry, Plasmonic nanofluids for high photothermal conversion efficiency in direct absorption solar collectors: fundamentals and applications, Solar Energy Mater. Solar Cells 201 (2019) 110084.
[38] M. Chen, Y. He, X. Wang, Y. Hu, Numerically investigating the optical properties of plasmonic metallic nanoparticles for effective solar absorption and heating, Solar Energy 161 (2018) 17–24.
[39] C.F. Bohren, D.R. Huffman, Absorption and scattering of light by small particles, 1998.
[40] C.L. Tien, B.L. Drolen, Thermal radiation in particulate media with dependent and independent scattering, Annual Rev. Heat Transf. 1 (1) (1987) 1–32.
[41] L. Wang, M. Wu, D. Wu, C. Zhang, Q. Zhu, H. Zhu, Optical absorption and photo-thermal conversion properties of CuO/H2O Nanofluids, J. Nanosci. Nanotechnol. 15 (4) (2015) 3178–3181.
[42] Y. Li, X. Zhao, P. Zhang, J. Ning, J. Li, Z. Su, G. Wei, A facile fabrication of large-scale reduced graphene oxide–silver nanoparticle hybrid film as a highly active surface-enhanced Raman scattering substrate, J. Mater. Chem. C 3 (16) (2015) 4126–4133.
[43] M. Chen, Y. He, J. Zhu, Preparation of Au–Ag bimetallic nanoparticles for enhanced solar photothermal conversion, Int. J. Heat Mass Transf. 114 (2017) 1098–1104.
[44] K. Wang, Y. He, A. Kan, W. Yu, D. Wang, L. Zhang, G. Zhu, H. Xie, X. She, Significant photothermal conversion enhancement of nanofluids induced by Rayleigh-Bénard convection for direct absorption solar collectors, Appl. Energy 254 (2019) 113706.
[45] R.M. Zhang, J. Qu, M. Tian, X.Y. Han, Q. Wang, Efficiency improvement of a solar direct volumetric receiver utilizing aqueous suspensions of CuO, Int. J. Energy Res. 42 (7) (2018) 2456–2464.
[46] L. Qiu, X. Zhang, Z. Guo, Q. Li, Interfacial heat transport in nano-carbon assemblies, Carbon N Y 178 (2021) 391–412.
[47] X.H. Zhang, G.E. Santoro, U. Tartaglino, E. Tosatti, Dynamical phenomena in fast sliding nanotube models, Philos. Mag. 93 (8) (2013) 922–948.
[48] H.E. Sauceda, I.L. Garzón, Structural determination of metal nanoparticles from their vibrational (Phonon) density of states, J. Phys. Chem. C 119 (20) (2015) 10876–10880.
[49] R. Meyer, D. Comtesse, Vibrational density of states of silicon nanoparticles, Phys. Rev. B 83 (1) (2011) 014301.
[50] G. Wu, B.W. Li, Thermal rectification in carbon nanotube intramolecular junctions: molecular dynamics calculations, Phys. Rev. B 76 (8) (2007).